



Modeling the edge effect for inverse determination of porous absorbers using feed forward neural networks

Mark Müller-Giebeler^{1,*}, Michael Vorländer¹

¹Institute for Hearing Technology and Acoustics, RWTH Aachen University
Kopernikusstraße 5, 52074 Aachen

*{mmg@akustik.rwth-aachen.de}

Abstract

Diffraction at the edges of finite absorber samples causes constructive as well as destructive interference and results in a sound field above the surface which deviates from the case of the infinitely extended material layer. This problem is referred to in the literature as finite sample effect or edge effect and is of importance in the context of free-field and in situ methods which attempt to derive material parameters from measurements of the total sound field (the so-called inverse wave field methods). The oscillations of the sound pressure around the reference curves are more pronounced the smaller the absorber sample. However, the exact values cannot be calculated in a simple way due to the complexity of the problem and the large number of influencing factors (material properties and geometry, position of source and receivers, frequency). This contribution presents preliminary work on the precise modeling of the edge effect based on supervised machine learning. In the context of this work it is discussed how FEM simulations have to be set up in principle in order to emulate the measurement of sound pressure over small absorbers in the semianechoic chamber as accurately as possible. Furthermore, it is shown how such simulations can be systematically varied in all relevant parameters to generate training data for artificial neural networks and how the network design and the actual training process are carried out.

Keywords: artificial neural networks, machine learning, sound field modeling, finite sample effect, porous materials

1 Introduction

Free-field and in-situ methods that attempt to derive the absorption coefficient, surface impedance or structural parameters of acoustic materials from sound field measurements above the absorber are the so-called acoustic field methods [1] or wave field analysis methods [2]. Within this category various approaches differ with respect to the physical quantities to be measured (sound pressure and/or particle velocity), certain basic assumptions about the wave field (plane wave or spherical wave hypothesis), the overall complexity of the measurement setup as well as the applied procedures for inversion of the underlying sound field model (simple calculation or complex iterative algorithms). However, a fundamental issue arises from the fact that practically all approaches are based on models of infinitely extended material layers or impedance planes and therefore diffraction occurring at the edges of finite absorber samples is not taken into account. The resulting constructive and destructive interferences lead to deviations from the reference sound field, which are more pronounced the smaller the sample under investigation [3, 4, 5]. This problem manifests itself in oscillations of the actual values of the sound field over the finite absorber around the reference curves for infinite material expansion. This discrepancy results in corresponding errors in the inverse determination of material parameters. Most attempts to address this issue are aimed at reducing or avoiding the influence of edge diffraction at the finite sample as well as possible, for example by clever positioning of the sensors or adjusting the height of the sound source [3, 4]. While these efforts only try to minimize the discrepancy between the actual measured values

and the models used, the aim of the approach presented here is to develop a universally applicable model for calculating the actual sound field, taking into account the edge effect, through training of multi-layered feed forward neural networks. Since there is no simple mathematical formulation for the sound field caused by a spherical wave over a finite absorber, specific cases are usually solved with numerical computational tools in forward simulations, i.e. the Boundary Element Method (BEM) or Finite Element Method (FEM). These calculations are in principle solutions of the Helmholtz equation taking into account various boundary conditions and parameters. Given that the universal approximation theorem states that already a network with only one hidden layer can approximate any continuous function [6, 7] provided that the network has enough hidden neurons and suitable activation functions, the results of numerical simulations are very well suited as training data for neural networks for generalized prediction of the sound field. The edge effect to be learned is formed as the sound pressure difference between the FEM simulations of finite absorber samples and an analytical model of infinite material extension. The systematically varied geometric and acoustically relevant model parameters serve as input features for the machine-learning model.

2 Method

In this section, the models and calculations used to determine the sound field contribution caused by the edge effect are introduced and the generation of training data based on them is described. Subsequently, the methodology of the design and training of the neural networks is discussed.

2.1. Theoretical model for the sound field above an infinite porous layer

The analytical model used in this work to calculate the sound field caused by a monopole source over a laterally infinite planar material surface is that of Allard et al. [8]. It predicts the velocity potential above a layer of porous material backed by an impervious surface using the two parameters $\nu_0^2 = (q^2 - k_0^2)$ and $\nu_m^2 = (q^2 - k_m^2)$ with $\text{Re}(\nu_0^2) > 0$ and $\text{Re}(\nu_m^2) > 0$ as follows:

$$\phi_{tot}(\vec{r}_s, \vec{r}_{rec}, k_0) = \frac{e^{-jk_0 R_{inc}}}{R_{inc}} - \frac{e^{-jk_0 R_{refl}}}{R_{refl}} + \int_0^\infty e^{-\nu_0(z_s+z_r)} \frac{2\rho_m}{\rho_m \nu_0 + \rho_0 \nu_m \tanh(\nu_m l)} J_0(qr) q dq \quad (1)$$

where $R_{inc} = \|\vec{r}_s - \vec{r}_{rec}\|$ is the distance between a source at \vec{r}_s and a receiver at \vec{r}_{rec} and $R_{refl} = \|\vec{r}_{is} - \vec{r}_{rec}\|$ is the distance between an image source at \vec{r}_{is} and the receiver. $J_0(x)$ represents the Bessel function of the first kind of order zero, r the horizontal distance between source and receiver and l the thickness of the material layer. Instead of a surface impedance value, the result only depends on the complex material parameters ρ_m and k_m , which are the effective density and wave number respectively. Therefore, no implicit assumptions are made about the material behavior and the model can effectively be used to calculate the sound field above a non-locally reacting material. The sound pressure $p_{tot}(\vec{r}_s, \vec{r}_{rec}, k_0)$ can then be evaluated from the equation

$$p_{tot}(\vec{r}_s, \vec{r}_{rec}, k_0) = -\rho_0 \frac{\delta \phi_{tot}}{\delta t} = j\omega \rho_0 \phi_{tot}(\vec{r}_s, \vec{r}_{rec}, k_0) \quad (2)$$

2.2. Johnson-Champoux-Allard equivalent homogeneous fluid model

In the context of this work, porous materials are generally modeled as an equivalent homogeneous fluid. All models belonging to this approach replace the complex two-phase poroelastic material by an equivalent damped fluid which adequately reflects the effective frequency-dependent propagation and energy dissipation in the material. Depending on the formulation, the models provide either the complex characteristic density $\underline{\rho}_m(\omega)$ that describes the visco-inertial effects and a dynamic bulk modulus $\underline{K}_m(\omega)$, describing the thermal effects within the porous medium or the combination of characteristic impedance $\underline{Z}_m(\omega)$ and propagation constant

$\underline{\Gamma}_m(\omega)$ of the equivalent fluid, both variants being easily convertible into each other:

$$\underline{Z}_m(\omega) = \sqrt{\underline{K}_m \underline{\rho}_m} \quad (3)$$

$$\underline{\Gamma}_m(\omega) = jk_m = j\omega \sqrt{\frac{\underline{\rho}_m}{\underline{K}_m}} \quad (4)$$

The well-established Johnson-Champoux-Allard model used here is one of the more complex poroacoustic models and is capable of describing sound propagation in porous media for a wide range of materials. In 1987, Johnson Koplik and Dashen proposed a semi-phenomenological expression of the effective density $\underline{\rho}_m(\omega)$ of a porous material considered to have a motionless skeleton and arbitrary pore morphologies [9]:

$$\underline{\rho}_m(\omega) = \frac{\alpha_\infty \rho_0}{\sigma} \left(1 + \frac{\Phi \sigma}{j\omega \rho_0 \alpha_\infty} \sqrt{1 + j \frac{4\alpha_\infty^2 \eta \rho_0 \omega}{\Phi^2 \Lambda^2 \sigma^2}} \right) \quad (5)$$

Later on Champoux and Allard expanded on that work and presented a model for the dynamic bulk modulus $\underline{K}_m(\omega)$ for the same type of material as follows[10]:

$$\underline{K}_m(\omega) = \frac{\frac{\gamma P_0}{\sigma}}{\gamma - (\gamma - 1) \left(1 - j \frac{8\eta}{\Lambda'^2 N_{Pr} \rho_0 \omega} \sqrt{1 + j \frac{\Lambda'^2 N_{Pr} \rho_0 \omega}{16\eta}} \right)^{-1}} \quad (6)$$

With the flow resistance Φ , the porosity σ , the tortuosity α_∞ and the viscous characteristic length Λ as well as thermal characteristic length Λ' , a total of 5 material parameters are required for the calculation. The constants are the viscosity of air ($\eta \approx 18.4 \cdot 10^{-6}$ Pa·s), the adiabatic index or heat capacity ratio ($\gamma = 1.4$), the standard atmospheric pressure ($P_0 = 101325$ Pa) and the Prandtl number ($N_{Pr} = 0.7179$) for air under standard conditions.

2.3. Problem Formulation: Modeling of the edge effect

As outlined in the introduction, the edge effect is understood as the sound field component caused by diffraction at a finite rectangular sample. Accordingly, for its calculation the differences are formed from the sound pressure values of the analytical model of Allard et al., assuming infinite material extension, and corresponding FEM simulation results of finite samples, as described in more detail in the following. All other parameters are the same in both calculation methods, which are also based on the identical material modeling of the absorber as an equivalent fluid according to the Johnson-Champoux-Allard model. The resulting complex-value difference values of the sound pressure between the analytical and numerical sound field computation ($\underline{p}_{Edge} = \underline{p}_{FEM} - \underline{p}_{Ana}$) constitute the target values to be learned by the supervised machine learning approach. The independent variables influencing the problem, i.e. the features of the machine learning model, are therefore on the one hand the geometrical parameters length, width and thickness of the material sample, as well as the source and receiver coordinates in space and on the other hand the 5 material parameters governing the poroacoustic model. A schematic representation of the entire data processing is shown in Figure 1.

2.4. Generation of Training Data using FEM simulations

For the calculation of sound fields over finite absorber samples, fully coupled FEM simulations were carried out, using the software COMSOL Multiphysics. Within the numerical model the porous material is equally parameterized as a homogeneous fluid according to the Johnson-Champoux-Allard model. As in the previously described analytical sound field model, which is based on a rigidly backed material layer, the ground is set to be ideally sound-hard in the FEM model. To ensure anechoic conditions at the remaining model boundaries, a Perfectly Matched Layer (PML) is added along the exterior. The basic structure of the FEM models is

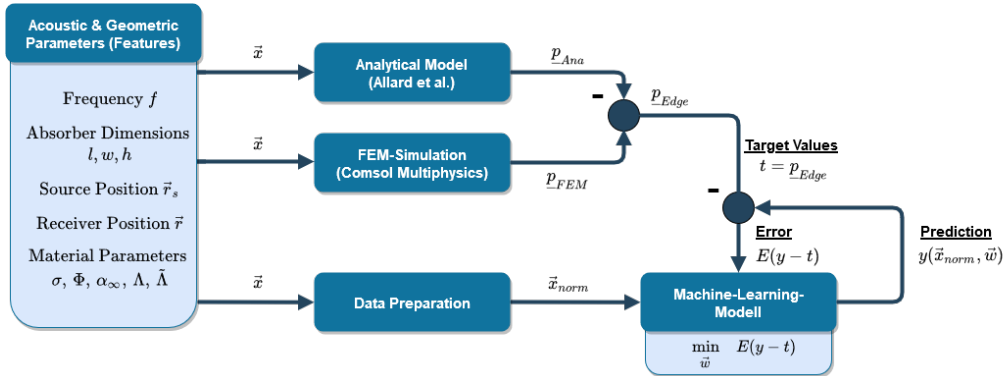


Figure 1: Flowchart for supervised learning of an ANN based on varied acoustic and geometric parameters as input variables. The prediction error is minimized by adjusting the model-specific weights.

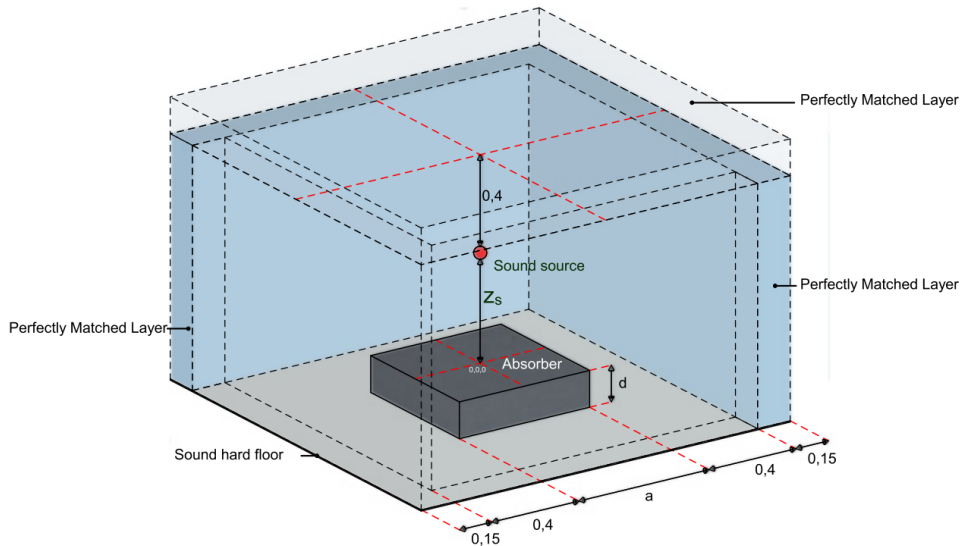


Figure 2: Exemplary sketch of a used FEM model with the dimensions of the rigidly backed absorber sample and the Perfectly Matched Layer (PML). The front and top sides of the PML are depicted transparently.

illustrated in Figure 2. Instead of a fixed spatial discretization, an adaptive frequency-dependent meshing was implemented. This allows the best possible reduction of the number of degrees of freedom and thus the total required computation time, while always maintaining the required numerical accuracy using triangular Lagrangian elements of quadratic order with a maximum element size of $\lambda/6$. As shown in the left block of the flowchart in Figure 1, the quantities affecting the result, i.e. the sound pressure value, include the frequency, the absorber dimensions, positions of source and receiver (3 Cartesian coordinates each) and the material parameters of the fluid model. This results in a total number of 15 parameters which are fed into the machine learning model as features and which have to be varied adequately in order to cover the feature space. (have to be varied in order to sufficiently cover the feature space). For this purpose, value arrays of length $N' = 100000$ (for an intended number of simulations N') were first generated for all parameters between a lower limit lb and an upper limit of parameter ub , with step size $(ub - lb)/(N' - 1)$. Subsequently, all parameter vectors were each randomly permuted and combined into a set of N' parameter combinations, which are fed to the FEM model. The interval limits used for the variation of the parameters or features can be found in Table 1. Due to the linear spacing in the output vector, the FEM simulations were based on equally distributed samples between respective lower and upper limits of all features. However, already the first training results showed that potential for the training of regression networks is wasted in this way, especially with respect to the parameter

Table 1: Parameters and associated interval limits for the simulation

Feature	lower bound lb	upper bound ub	unit
Frequency f	50	1200	Hz
Sample length and width l, w	0.2	1.0	m
sample height h	0.01	0.25	m
x- and y-coordinate receiver x, y	-0.25	0.25	m
z-coordinate receiver z	0.02	0.2	m
x- and y-coordinate source x_s, y_s	-0.25	0.25	m
z-coordinate source z_s	0.3	0.8	m
Flow resistivity Φ	500	1.5E6	$\frac{\text{Pa s}}{\text{m}^2}$
Porosity σ	0.005	0.995	-
Tortuosity α_∞	1	4	-
Viscous Characteristic Length Λ	5	400	μm
Thermal Characteristic Length Λ'	5	800	μm

flow resistance. This could be seen from the fact that sound field results calculated with the trained networks for materials with low flow resistivity were also promising, but were still significantly less accurate than those for large values of flow resistivity. This relationship can also be easily plausibilized by sensitivity analyses on the influence of the individual material parameters, which show that the variance of resulting sound pressure results is large for small flow resistivities and decreases with increasing absolute value of the material parameter. Therefore, to better sample this feature when generating training data, a second set of $N'' = 50000$ simulations was added based on a vector of logarithmically spaced points between the previously used flow resistivity interval boundaries. Finally, the two data sets were combined into a number of $N = N' + N'' = 150000$ training data. Another combination of 30000 results of logarithmically spaced and 60000 linearly spaced flow resistivity vectors served as test data set. The systematic script-based parameterization and execution of the extensive simulation series could be comfortably implemented using the LiveLink for MATLAB function of COMSOL.

2.5. Network Design / Architecture and Learning of NN

One type of neural networks that are frequently used for function approximation are multilayer feedforward neural networks trained with the backpropagation algorithm. This type of network consists of an input layer, an output layer, and at least one hidden layer, each with an arbitrary number of neurons. The neurons are the nodes of a graph and have connections (edges) to all neurons of the respective previous and subsequent layer (with the exception of the bias nodes, which only have outgoing connections). Such layers are also called fully connected layers and represent the standard case for neural networks. The strength of the connection between two neurons is quantified by the edge weights, the coefficients that are optimized during training. The outputs of a feedforward neural network for regression with two layers (the input layer is not counted) can be written as

$$y_k = g_2 \left(\sum_{j=1}^M w_{kj} g_1 \left(\underbrace{\sum_{i=1}^D w_{ji} x_i + w_{j0}^{(1)}}_{=z_j} \right) + w_{k0}^{(2)} \right) \quad (7)$$

where y_k is the k^{th} output, g_1 and g_2 the activation functions, $w_{i,j}$ the edge weight from node i to node j , x_i the i^{th} input and $w_{j0}^{(1)}$ and $w_{k0}^{(2)}$ the corresponding bias weights for layer 1 and 2 respectively. The network topology representation corresponding to the function is shown in Figure 3. In this work, networks with up to three hidden layers are studied. Since the benefit of Rectified Linear Unit (ReLU) activations in terms of more stable gradients during backpropagation is hardly given for shallow networks, hyperbolic tangent activations

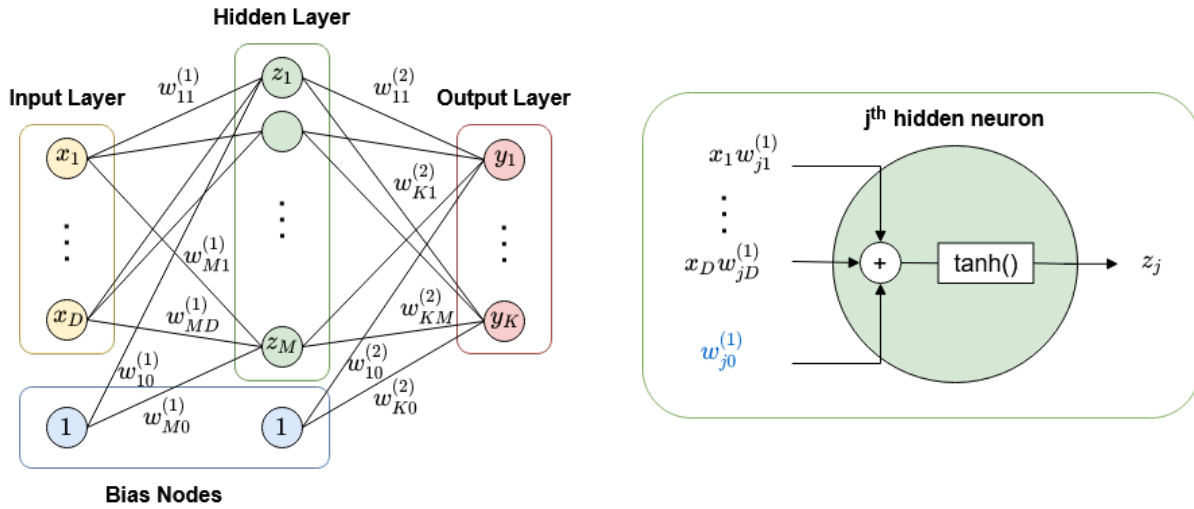


Figure 3: Illustration of a two-layer neural network with D inputs, M hidden neurons (each using hyperbolic tangent activation functions), and K outputs. The bias nodes (filled in blue) have no incoming connections.

for the hidden layers were used instead in combination with linear activations for the output layer. The learning process during training is generally considered as the iterative optimization of the network weights and biases with respect to an appropriate cost function. In this case, the performance function used is the mean squared error (MSE), which is defined as

$$MSE = \frac{1}{K} \frac{1}{N} \sum_{k=1}^K \sum_{n=1}^N (t_{n,k} - y_k(\vec{x}_n, \vec{w}))^2 \quad (8)$$

with $K = 2$ network outputs, namely the real and imaginary parts of the sound pressure and a set of $N = 150000$ training data points. For the Training of the networks, the Levenberg-Marquardt algorithm was chosen. Although it is considered to be relatively memory demanding compared to other training functions, it has the advantage of significantly faster convergence, especially for problems of accurate function approximation by networks with a limited number of weights. For shallow backpropagation networks, the initial weights and bias values for a layer are computed in Matlab using the Ngyuen-Widrow method, which generates the initial values such that the active regions of the neurons are approximately evenly distributed across the layer's input space [11]. While still maintaining a certain degree of randomness, the main advantage over purely random weights and biases is a significant speedup of the training process. For the purpose of preventing the neural networks from overfitting, the early stopping method was applied during training. This requires splitting the data set into a training set, used to minimize the cost function (eq. 8) and a validation set, used to evaluate the current network during training with unknown data. Therefore, this subset is not learned directly but acts as a regularization. While the training error decreases as optimization progresses, it is possible that the validation error increases again due to overfitting after an optimum is reached. The goal of early stopping is now to stop training as soon as the validation error has reached its minimum, which usually results in a well-adapted network with good generalization capabilities. Since only approximations of the gradients or the Hessian matrix are used in the optimization, noise in the minimization process could lead to a premature termination. Therefore, a threshold value of 10 successive increases of the validation error was defined as a termination criterion. For the final verification and evaluation of the model with completely unknown data, a third set of data is used, the so-called test data set.

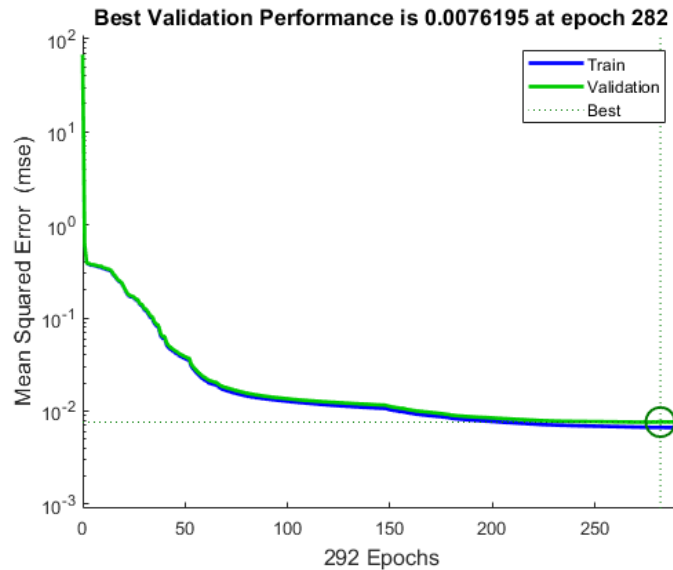


Figure 4: Progression of training and validation errors to the time of termination due to early-stopping.

3 Results

In the upcoming extensive studies, the best combination of number of layers and number of neurons will be determined by extensive comparative studies. As an example and proof of concept, only the training results and performance of a neural network with 3 hidden layers with 70, 50 and 30 neurons are evaluated below. This is the topology that achieved the best results in the limited pre-study presented here. The training was terminated due to early-stopping after 292 epochs and the performance measure, i.e. the mean square error (MSE), for this network is 0.0069. The training and validation error curves are shown in Figure 4. The final evaluation of performance is based on the completely unknown test data set of 90000 additional simulation results. The correlation between sound pressure prediction by the trained network and the reference values according to FEM are shown in Figure 6 (real part) and Figure 7 (imaginary part), respectively. Also plotted are the histograms of the relative prediction errors, each in comparison to the analytical model according to Allard et al. Even if there are still deviations from the reference results of the FEM simulations in some cases, a clear improvement of the calculation of the sound field over finite absorber samples is clearly visible. To make the training results more descriptive with respect to acoustic practice, Figure 5. shows a simulated sweep measurement of the total sound pressure at a receiver position at a height of 5 cm centered over a small absorber sample (L x W x H = 30 cm x 50 cm x 20 cm).

4 Discussion and Outlook

In this work, the training of artificial neural networks for modeling the edge effect over finite porous absorber samples was presented. At least for certain applications (e.g. inverse material characterization methods) and within the previously chosen parameter and modeling limits, neural network based sound field modeling has the potential to completely replace less suitable analytical models on the one hand or computationally much more complex numerical simulations on the other hand. The effort required to generate the corresponding training data is justified, especially with regard to problems that require a large number of model evaluations (parameter studies, iterative procedures, etc.). Note that the specification of the 5 material parameters of the JCA model as features is simply due to the fact that the networks trained here are to be used first in the context of an approach for the inverse estimation of exactly these frequency-independent porous material parameters. Instead, it is equally possible to choose the general parameters of the fluid medium (e.g., $\rho_m(\omega)$ and $k_m(\omega)$) as input features of the neural networks, which does not change the conceptual approach described in this

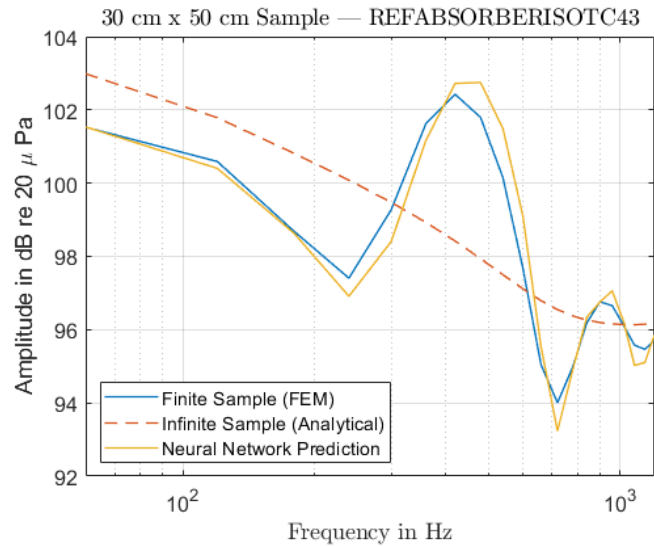


Figure 5: Sound pressure level (showing pronounced edge effect) evaluated at a height of $z_r = 0.05$ m centered above a porous material sample (0.3 m x 0.5 m x 0.2 m). Comparison between the exact FEM results, the analytical model of infinite material extension and the neural network prediction.

paper. Both variants of implementation will be studied in detail as part of the following work. Approaches to further improve the performance of the networks are to investigate other network topologies and complexities, to increase the number of training data used, and to penalize deviations from the target values for smaller flow resistivity values more strongly during training by using appropriate error weights.

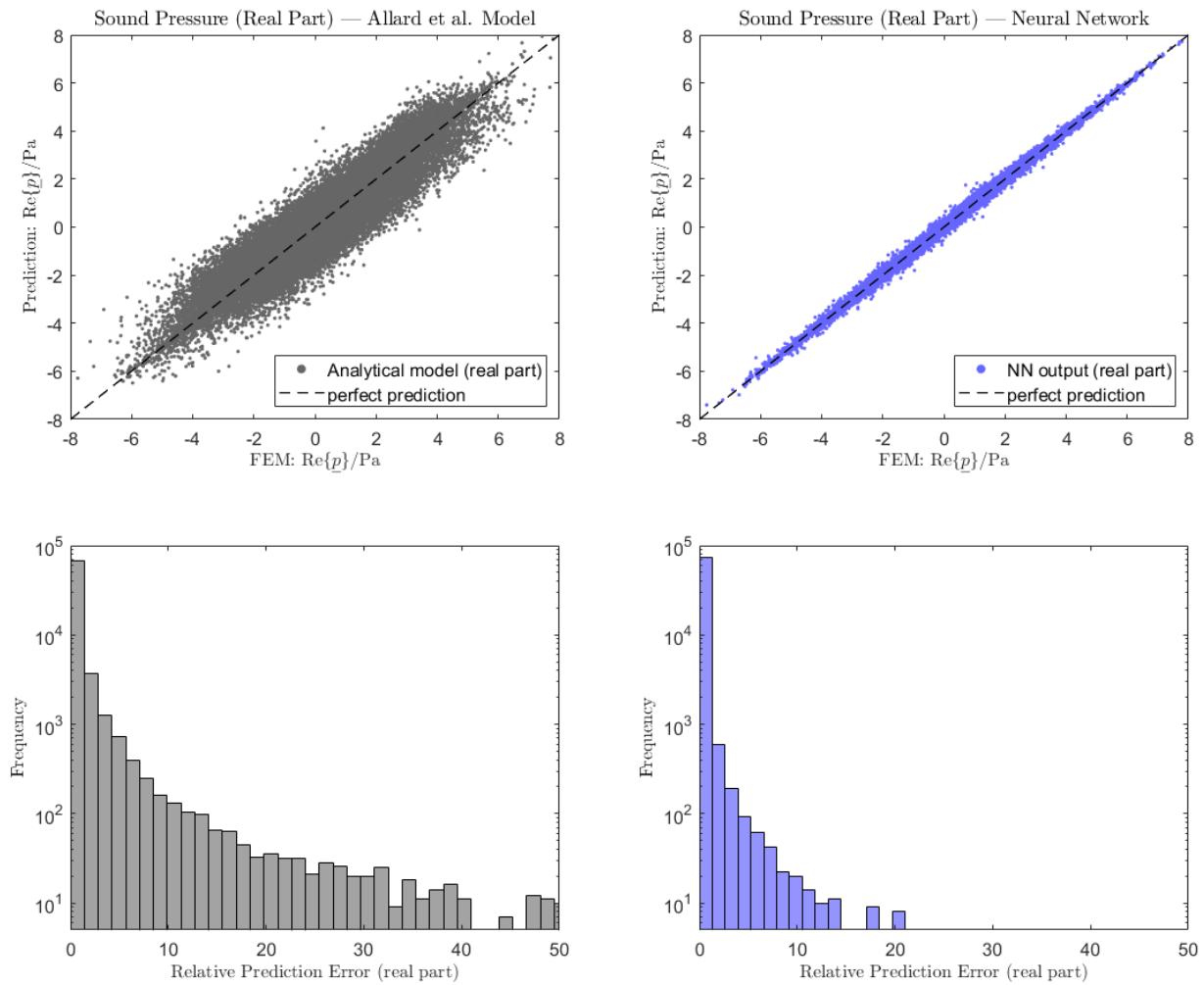


Figure 6: **Upper row:** Comparison of the sound pressure predictions (real part) of the Allard et. al model and the four-layer neural network (70x50x30 hidden neurons), each plotted against the corresponding FEM values. **Bottom row:** comparison of histograms of the two error distributions with logarithmically scaled ordinate.

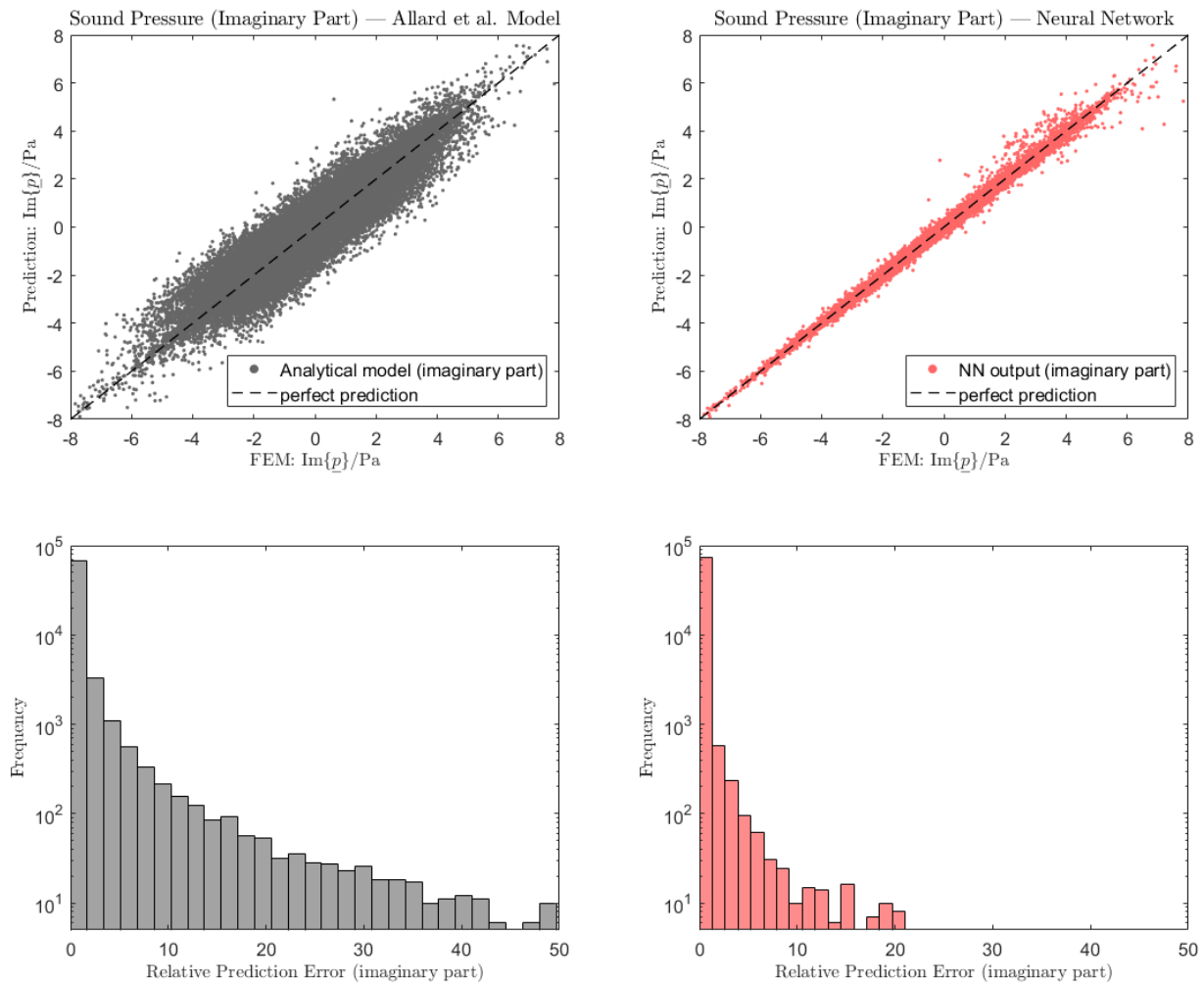


Figure 7: **Upper row:** Comparison of the sound pressure predictions (real part) of the Allard et. al model and the four-layer neural network (70x50x30 hidden neurons), each plotted against the corresponding FEM values. **Bottom row:** comparison of histograms of the two error distributions with logarithmically scaled ordinate.

References

- [1] Eric Brandão, Arcanjo Lenzi, and Stephan Paul. A review of the *In Situ* impedance and sound absorption measurement techniques. 101(3):443–463, 2015.
- [2] Lieven De Geetere. Analysis and improvement of the experimental techniques to assess the acoustical reflection properties of boundary surfaces, 2004.
- [3] Eric Brandão, Arcanjo Lenzi, and Julio Cordioli. Estimation and minimization of errors caused by sample size effect in the measurement of the normal absorption coefficient of a locally reactive surface. 73(6-7):543–556, 2012. PII: S0003682X11002672.
- [4] Kunikazu Hirosawa, Kazuhiro Takashima, Hiroshi Nakagawa, Makoto Kon, Aki Yamamoto, and Walter Lauriks. Comparison of three measurement techniques for the normal absorption coefficient of sound absorbing materials in the free field. 126(6):3020–3027, 2009. Journal Article.
- [5] Toru Otsuru, Reiji Tomiku, Nazli Bin Che Din, Noriko Okamoto, and Masahiko Murakami. Ensemble averaged surface normal impedance of material using an in-situ technique: preliminary study using boundary element method. 125(6):3784–3791, 2009. Journal Article Research Support, Non-U.S. Gov't.
- [6] Kurt Hornik, Maxwell Stinchcombe, and Halbert White. Universal approximation of an unknown mapping and its derivatives using multilayer feedforward networks. 3(5):551–560, 1990. PII: 0893608090900056.
- [7] Moshe Leshno, Vladimir Ya. Lin, Allan Pinkus, and Shimon Schocken. Multilayer feedforward networks with a nonpolynomial activation function can approximate any function. 6(6):861–867, 1993. PII: S0893608005801315.
- [8] Jean-François Allard, Walter Lauriks, and Christine Verhaegen. The acoustic sound field above a porous layer and the estimation of the acoustic surface impedance from free-field measurements. 91(5):3057–3060, 1992.
- [9] David Linton Johnson, Joel Koplik, and Roger Dashen. Theory of dynamic permeability and tortuosity in fluid-saturated porous media. *Journal of Fluid Mechanics*, 176(-1):379, 1987.
- [10] Yvan Champoux and Jean-F. Allard. Dynamic tortuosity and bulk modulus in air-saturated porous media. *Journal of Applied Physics*, 70(4):1975–1979, 1991.
- [11] D. Nguyen and B. Widrow. Improving the learning speed of 2-layer neural networks by choosing initial values of the adaptive weights. In *1990 IJCNN International Joint Conference on Neural Networks*, pages 21–26 vol.3. IEEE, 6/17/1990 - 6/21/1990.